PHOTOCATALYSIS

1. Introduction

Heterogeneous photocatalysis is a discipline that includes a large variety of reactions: mild or total oxidations, dehydrogenation, hydrogen transfer, oxygen-18 and deuterium isotopic exchange, metal deposition, water detoxification, gaseous pollutant removal, bactericidal action, etc. Bactericidal action can be considered as one of the new Advanced Oxidation Technologies (AOT) for air and water purification treatments. Several books and reviews have been recently devoted to AOT (1–11). A recent review has reported more than 1200 references on the subject (11).

As heterogeneous catalysis, photocatalysis can be carried out in various media : gas phase, pure organic liquid phases or aqueous solutions. As for classical heterogeneous catalysis, the overall process can be broken down into five independent steps :

1. Transfer of the reactants in the fluid phase to the surface.
2. Adsorption of at least one of the reactants.
3. Reaction in the adsorbed phase.
4. Desorption of the product(s).
5. Removal of the products from the interface region.

The only difference with conventional catalysis is the mode of activation of the catalyst in which the thermal activation is replaced by a photonic activation. The activation mode is not concerned with steps 1, 2, 4 and 5, although photoadsorption and photodesorption of some reactants, mainly oxygen, do exist. Step 3 contains all the photoelectronic processes and can be broken down as follows:

3.1 **AB**sorption of the photons *by the solid and not by reactants*. There is no photochemistry in the adsorbed phase.
3.2 Creation of electron-hole pairs that dissociate into photoelectrons and positive photo-holes (electron vacancies).
3.3 Electron transfer reactions such as ionosorption (eg, O_2, NO, etc), charge neutralization, radical formation, surface reactions, etc.

2. Principles of Heterogeneous Photocatalysis

When a semiconductor catalyst, SC, of the chalcogenide type, oxides (TiO_2, ZnO, ZrO_2, CeO_2), or sulfides (CdS, ZnS) is illuminated with photons whose energy is equal to or greater than their band-gap energy E_G ($h\nu \geq E_G$), there is **AB**sorption of these photons and creation within the bulk of electron-hole pairs, which dissociate into free photoelectrons in the conduction band and photoholes in the valence band (Fig. 1).

Simultaneously, in the presence of a fluid phase (gas or liquid), a spontaneous **AD**sorption occurs and according to the redox potential (or energy level)

of each adsorbate, an electron transfer proceeds towards acceptor molecules, whereas a positive photohole is transferred to a donor molecule. Actually the hole transfer corresponds to the cession of an electron by the donor to the solid.

$$h\nu + (\mathrm{SC}) \rightarrow e^- + h^+ \quad (1)$$

$$\mathrm{A}_{(\mathrm{ads})} + e^- \rightarrow \mathrm{A}^-_{(\mathrm{ads})} \quad (2)$$

$$\mathrm{D}_{(\mathrm{ads})} + h^+ \rightarrow \mathrm{D}^+_{(\mathrm{ads})} \quad (3)$$

Each ion formed subsequently reacts to form the intermediates and final products. As a consequence of reactions 1–3, the photonic excitation of the catalyst appears as the initial step of the activation of the whole catalytic system. Thence, the efficient photon has to be considered as a reactant and the photon flux as a special fluid phase, the "electromagnetic phase". The photon energy is adapted to the absorption by the catalyst, not to that of the reactants. The activation of the process goes through the excitation of the solid but not through that of the reactants : *there is no photochemical process in the adsorbed phase* but only a true heterogeneous photocatalytic regime as demonstrated further.

The photocatalytic activity or the quantum yield defined later in section 5.6, can be reduced by the electron-hole recombination, described in Fig. 2, which corresponds to the degradation of the photoelectonic energy into heat.

$$e^- + h^+ \longrightarrow \mathrm{N} + \mathrm{E} \quad (4)$$

where N = neutral center; E = energy (light $h\nu' \leq h\nu$ or heat).

3. Catalysts

Various chalcogenides (oxides and sulfides) have been used: TiO_2, ZnO, CeO_2, ZrO_2, SnO_2, $SbrO_4$ CdS, ZnS, etc. As generally observed, the best photocatalytic performances with maximum quantum yields are always obtained with titania. In addition, anatase is the most active allotropic form among the various ones available, either natural (rutile and brookite) or artificial (TiO_2-B, TiO_2-H). Anatase is thermodynamically less stable than rutile, but its formation is kinetically favored at a lower temperature (<600°C). This lower temperature could explain a higher surface area, and surface density of active sites for adsorption and for catalysis. In all the systems described in this article, the catalyst used was titania (Degussa TiO_2 P-25, 50 m^2/g, mainly anatase), unless otherwise stated.

Titania was sometimes modified either by ion doping or by deposition of a metal (Pt, Rh or Ni). In the latter case, the metal was deposited by impregnation of TiO_2 Degussa P-25 with a metal salt followed by drying and reduction under hydrogen flow at 400°C. Homogeneously-doped TiO_2 samples were obtained in a flame reactor by oxidation at high temperature of a solution of the heterocation chloride in liquid $TiCl_4$ (13). This was the best means of obtaining a constant concentration of doping agents as a function of the distance from the surface to the center of the bulk of catalysts' particles.

4. Photoreactors

Depending on the reaction considered, fixed-bed photoreactors or slurry batch photoreactors either mechanically or magnetically stirred can be chosen.

For laboratory experiments, near-uv light was provided by a Philips lamp (HPK 125 watts) placed in front of an the optical window of the photoreactor. Ir beams were removed by a circulating-water cell. The wavelength was adjusted with optical filters (fused silica, or Pyrex, or Corning glass filters) (Fig. 3). The radiant flux was measured with a radiometer (Radiometer Technology model 21A) calibrated against a calorimeter.

For solar photocatalytic detoxification, the experimental pilot photoreactor of PSA was used, which has been thoroughly described by Malato (14–16).

5. Influence of the Five Basic Physical Parameters Governing the Kinetics

All the results presented in this section are summarized in Fig. 4.

5.1. Mass of Catalyst. Either in static, slurry, or dynamic flow photoreactors, the initial rates of reaction were found to be directly proportional to the mass m of catalyst (Fig. 4**a**). This indicates a true heterogeneous catalytic regime. Actually, the reaction rate r is proportional to the true rate constant k and to the total number of active sites n_T given by :

$$r = kn_T = k \times d \times m \times S_{BET} \tag{5}$$

where d is the mean active site surface density, m is the mass of catalyst employed and S_{BET} is the specific aera of the catalyst.

However, above a certain value of m, the reaction rate levels off and becomes independent of m. This limit depends on the geometry and on the working conditions of the photoreactor. These limits correspond to the maximum amount of TiO_2 in which all the particles, ie, all the surface exposed are totally illuminated. For higher quantities of catalyst, a screening effect of excess particles occurs, which masks part of the photosensitive surface. For applications, this optimum mass of catalyst has to be chosen in order (*1*) to avoid an unuseful excess of catalyst and (*2*) to ensure a total absorption of efficient photons. These limits range from 0.2 to 2.5 g/L of titania in slurry batch photoreactors.

5.2. Wavelength. The variations of the reaction rate as a function of the wavelength follows the absorption spectrum of the catalyst (Fig. 4**b**), with a threshold corresponding to its band gap energy. For TiO_2 having $E_G = 3.02$ eV, this requires: $\lambda \leq 400$ nm, ie, near-uv wavelengths (uv-A). In addition, it must be checked that the reactants do not absorb the light to conserve the exclusive photoactivation of the catalyst for a true heterogeneous catalytic regime (no homogeneous or photochemistry in the adsorbed phase). Since the solar spectrum contains 3–5% Uv-energy, photocatalysis can be activated by solar energy ("Helio-photocatalysis").

5.3. Initial Concentration and/or Partial Pressure of Reactants. Generally, the kinetics follows a Langmuir-Hinshelwood mechanism confirming the heterogeneous catalytic character of the system with the rate r varying proportionally with the coverage θ as:

$$r = k\theta = k(KC/(1+KC)) \tag{6}$$

where k is the true rate constant, K is the constant of adsorption at equilibrium, and C is the instantaneous concentration.

For diluted solutions ($C < 10^{-3}$ M), KC becomes $\ll 1$ and the reaction is of the apparent first order, whereas for concentrations $> 5 \times 10^{-3} M$, ($KC \gg 1$), the reaction rate is maximum and is of the apparent order (Fig. 4**c**).

In the gas phase, similar Langmuir-Hinshelwood expressions have been found including partial pressures P instead of C.

$$r = k\theta = k(KP/(1+KP)) \tag{7}$$

In some cases, such as in liquid alcohol dehydrogenation (17,18), the rate follows variations including the square root of concentration:

$$r = k\left[K^{1/2}C^{1/2}/\left(1+K^{1/2}C^{1/2}\right)\right] \tag{8}$$

This indicates that the active form of the reactant is in a dissociated adsorbed state. In other cases, such as in the photocatalytic degradation and mineralization of chlorobenzoic acids (19), a zero kinetic order was found, even at low concentrations. This was due to a strong chemisorption on titania with the saturation of the hydroxylic adsorption sites. For a maximum reaction rate and correlatively for the highest quantum yield, reactions should be performed with initial concentrations equal to or higher than the threshold of the plateau ($C_o \geq$ ca. $5 \times 10^{-3} M$).

5.4. Temperature. Because of the photonic activation, the photocatalytic reactions do not require heating and are operating at room temperature. The true activation energy, E_t, relative to the true rate constant k ($k = k_0$ exp $(-E_C/RT)$) is nil, whereas the apparent activation energy, E_a, is often very small (a few kJ/mol) in the medium temperature range ($20^\circ C \leq \theta \leq 80^\circ C$). However, at very low temperatures ($-40^\circ C \leq \theta^\circ C \leq 0^\circ C$), mainly for gas phase reactions, the activity decreases and the activation energy, E_a, becomes positive (Fig. 4**d**). By contrast, at "high" temperatures ($\theta^\circ C \geq 70-80^\circ C$) for various types of photocatalytic reactions, the activity decreases and the apparent activation energy becomes negative (Fig. 4**c**).

This behavior can be easily explained within the frame of the Langmuir-Hinshelwood mechanism described above. The decrease in temperature favors adsorption which is a spontaneous exothermic phenomenon. Coverage θ tends to unity, whereas KC becomes $\gg 1$. In addition, the lowering in T also favors the adsorption of the final reaction product P, whose desorption tends to inhibit the reaction. Correspondingly, there appears a term $K_P C_P$ in the denominator of eq. 5. If P is a strong inhibitor, one gets: $K_P C_P \gg (1+KC)$ and the Langmuir-

Hinshelwood equation becomes:

$$r = k\theta = kKC/(1 + KC + K_{\mathrm{P}}C_{\mathrm{P}}) \approx kKC/K_{\mathrm{P}}C_{\mathrm{P}} \tag{9}$$

where Kp is the adsorption constant of final product P. There results an apparent activation energy E_{a} equal to:

$$E_{\mathrm{a}} = E_{\mathrm{t}} + \Delta H_{\mathrm{A}} - \Delta H_{\mathrm{P}} \tag{10}$$

ie, to the algebraic sum of the true activation energy E_{t} (theoretically equal to zero) and of the enthalpies of adsorption ΔH_{A} and ΔH_{P} of reactant A and of the inhibiting final product P, respectively. Since ΔH_is are always negative, one generally write : $\Delta H_i = -Q_i$, Q_i being the heat of adsorption of compound i and counted positive.

$$E_a = E_t - Q_A + Q_P \approx 0 - Q_A + Q_P = -Q_A + Q_P \tag{11}$$

If product P is a strong inhibitor, this means that $Q_{\mathrm{A}} < Q_{\mathrm{P}}$ in eq. 10 and that E_a tends asymptotically to Q_P. Such a relationship was actually verified for photocatalytic reactions involving hydrogen, mainly alcohol dehydrogenation (17,18) and alkane-deuterium isotopic exchange (20,21), the latter reaction being used to characterize active sites in catalysis by metals (22–25).These reactions were carried out on bifunctional Pt/TiO_2 photocatalysts prepared by impregnation of the support by H_2PtCl_6 and subsequent reduction by hydrogen (17,18). E_a was found equal to $+10$ kcal/mol ($+42$ kJ/mol), which equals the adsorption heat $Q_{H_2}(\mathrm{ads})$(or to the opposite of the enthalpy $\Delta H_{H_2(\mathrm{ads})}$) of reversibly adsorbed hydrogen on platinum, measured by microcalorimetry (26).

$$E_a = E_t - \Delta H_{H_2(\mathrm{ads})} = 0 + Q_{H_2(\mathrm{ads})} = +10\,\mathrm{kcal/mol}(42\mathrm{kJ/mol}) \tag{12}$$

Actually, this behavior where E_a tends to Q_P was only observed -up to now- for bifunctional Pt/TiO_2 photocatalysts.

On the other hand, when θ°C increases above 80°C and tends to the boiling point of water, the exothermic adsorption of reactant A becomes disfavored and tends to limit the reaction. Consequently, the Langmuir-Hinshelwood equation becomes:

$$r = \mathrm{k}\theta = kKC/(1 + KC) \approx k\,KC \tag{13}$$

with an apparent activation energy equals to :

$$E_a = E_t + \Delta H_A \tag{14}$$

As the temperature increases, the adsorption of reactant A becomes limited (27) and E_a, which is now negative, tends to $-Q_A$

$$E_a = E_t + \Delta H_{\mathrm{A}} \approx 0 + \Delta H_{\mathrm{A}} = -Q_{\mathrm{A}} < 0 \tag{15}$$

As a consequence, the optimum temperature is generally comprised between 20 and 80°C. *This explains why those of solar devices which use light concentrators instead of light collectors require coolers* (28). This absence of heating is attractive for photocatalytic reactions carried out in aqueous media and in particular for environmental purposes (photocatalytic water purification). There is no need to waste energy in heating water which possesses a high heat capacity. This is the reason why photocatalysis is cheaper than incineration (29).

5.5. Radiant Flux. It has been shown, for all types of photocatalytic reactions, that the rate of reaction r is proportional to the radiant flux Φ (Fig. 4**e**). This confirms the photo-induced nature of the activation of the catalytic process, with the participation of photo-induced electrical charges (electrons and holes) to the reaction mechanism. However, above a certain value, estimated to be ca. 25 mW/cm^2 in laboratory experiments performed on the photoreactor in Fig. 3, the reaction rate r becomes proportional to $\Phi^{1/2}$. This can be demonstrated as follows.

Moderate Radiant Fluxes. The five basic equations (see section 2) are

$$(TiO_2) + hv \longrightarrow e^- + h^+ \tag{16}$$

$$e^- + h^+ \longrightarrow \mathrm{N} + \text{energy} \tag{17}$$

$$\mathrm{A} + e^- \longrightarrow \mathrm{A}^- \tag{18}$$

$$\mathrm{D} + h^+ \longrightarrow \mathrm{D}^+ \tag{19}$$

$$\mathrm{A}^- + \mathrm{D}^+ \longrightarrow \text{Intermediate products} \tag{20}$$

and the rate limiting step is the reaction in the adsorbed phase (eq. 20). Therefore

$$r = r_{18} = k_{18}[A^-][D^+] \tag{21}$$

In an n-type semiconductor such as titania, the photo-induced holes are much less numerous than electrons (photo-induced electrons plus n-electrons): $[h^+] \ll [e^-]$. Therefore holes are the limiting active species. Thence:

$$r = r_{18} = r_{17} = k_{17}[D][h^+] \tag{22}$$

At any instant, one has:

$$d[h^+]/dt = r_{14} - r_{15} - r_{17} = 0 = k_{14} - k_{15}[e^-][h^+] - k_{17}[D][h^+] \tag{23}$$

Thence:

$$[h^+] = \frac{K_{14}\Phi}{k_{15}[e^-] + k_{17}[D]} \tag{24}$$

and

$$r = \frac{k_{17}[D]k_{14}\,\Phi}{k_{15}[e^-] + k_{17}[D]} = \frac{k_{14}\,k_{17}[D]\Phi}{k_{17}[D] + k_{15}[e^-]} \propto \Phi \tag{25}$$

From the above equation, it can be seen that the reaction rate is directly proportional to the radiant flux Φ.

High Radiant Fluxes. In the case of high fluxes, the instantaneous concentrations $[e^-]$ and $[h^+]$ strongly increase and $k_{15}[e^-]$ becomes much larger than $k_{17}[D]$. Therefore, eq. (23) becomes:

$$[h^+] \approx K_{14}\,\Phi/k_{15}[e^-] \qquad \text{with } [h^+] \approx [e^-] \tag{26}$$

Thence

$$[h^+]^2 \approx k_1\,\Phi/k_2 \tag{27}$$

The reaction rate r becomes

$$r = r_{18} = r_{17} = k_{17}[D](k_{14}\Phi/k_{15})^{1/2} \propto \Phi^{1/2} \tag{28}$$

indicating that r has become proportional to $\Phi^{1/2}$ and that the rate of electron-hole formation becomes greater than the photocatalytic rate, which favours the electron-hole recombination (eq. 16). In any photocatalytic device, the optimal light power utilization corresponds to the domain where r is proportional to Φ.

5.6. Photocatalytic Quantum Yield (or Quantum Efficiency). By definition, it is equal to the ratio of the reaction rate in molecules converted per second (or in mols per second) to the incident efficient photonic flux in photons per second (or in Einstein per second (an Einstein is a mol of photons)). This is a kinetic definition, which is directly related to the instantaneous efficiency of a photocatalytic system. Its theoretical maximum value is equal to 1. It may vary on a wide range according (*1*) to the nature of the catalyst; (*2*) to the experimental conditions used (concentrations, T, m, etc) and (*3*) especially to the nature of the reaction considered. The values found were comprised between 10^{-2} % and 70%. This highest value was observed in the case of methanol dehydrogenation over Pt/TiO_2 (0.5 wt % Pt) in pure liquid phase (18). The knowledge of this parameter is fundamental. It enables one (*1*) to compare the activity of different catalysts for the same reaction, (*2*) to estimate the relative feasability of different reactions, and (*3*) to calculate the energetic yield of the process and the corresponding cost.

5.7. Influence of Oxygen Pressure in Oxidation Reactions. It could be easily determined in gas phase reactions. For instance, in the mild photocatalytic oxidation of alkanes into aldehydes and/or ketones, it was found that the kinetic order of oxygen was nil, indicating a total surface coverage of this gas (30). Photoconductivity measurements indicated that oxygen was photoadsorbed as two forms O^- and O_2^-(30). For liquid phase reactions, it was difficult to study the influence of PO_2 because the reaction is polyphasic. It is generally assumed that oxygen adsorbs on titania from the liquid phase, where it is dissolved following Henry's law. If the oxygen is regularly supplied, from the gas phase (often air) it can be assumed that its coverage θ_{O_2} at the surface of titania

is constant and can be integrated into the apparent rate constant:

$$A + O_2 \longrightarrow P \tag{29}$$

$$r_A = -d[A]/dt = k\theta_A\theta_{O_2} = k_{app}\theta_A \tag{30}$$

Experiments on titania's photocatalytic activity as a function of PO_2 between 1/5 and 5 atmospheres (ie, between 20 and 500 kPa) did not indicate any variation of the reaction rate.

6. Considerations on the Fate of Photo-holes, h^+, in Titania

As demonstrate above, uv-light absorption by titania creates photo-electrons and holes, the latter being strong oxidizing agents. The simultaneous existence of both e^- and h^+ electrical charges implies the existence of redox processes.

Since electrons are more numerous than holes because of the *n*-type semiconductor character of titania, holes represent the limiting species in photocatalytic processes. Physically, holes are electron vacancies and are, therefore, virtual positive electrical charges. Physicists consider them as positive and mobile charges, whose motion in the solid is ensured by their filling with electrons arising from a neighboring anion O^{2-}. The chemical support of the hole, h^+, in the valence band is a lattice anion, O_L^-.

Therefore, the migration of holes in the bulk can be written as:

$$O_L^- + O_L^{2-} \longrightarrow O_L^{2-} + O_L^-$$

or

$$h^+ + O_L^{2-} \longrightarrow O_L^{2-} + h^+$$

This motion of holes ensures an electrical conductivity by a "hopping type".

Therefore, the fate of photo-holes h^+ is of a paramount importance for photocatalysis. Several options are possible.

6.1. Direct Electron-hole Recombination. The corresponding reaction is given by the equation 4.

This is a highly exothermic reaction, which restitutes most of the 3.2 eV of the gap energy E_G absorbed by the solid. It is of the second order kinetics, which means that it strongly increases with the square of the charge concentrations.

This is why it is reasonable to work at and/or below the optimum value of the radiant flux given in Fig. 4**e**. This value depends on the irradiation power source and on the design of the photoreactor.

6.2. Indirect Electron-hole Recombination. The consumption of holes can be induced by cationic impurities, which, if they are controlled, can be defined as doping agents. They must be heterovalent with respect to Ti^{4+} cations, ie, having a valency equal to 4 ± 1.

n-Type Doping. *n*-Type doping corresponds to the dissolution of pentavalent (Nb^{5+}, Ta^{5+}, Sb^{5+}), [even hexa-(Mo^{6+}) and hepta-valent (Re^{7+})] cations in

the lattice positions of Ti^{4+} which creates donor centers according to:

$$[(M^{5+})e^-] \rightleftharpoons (M^{5+}) + e^-$$

or

$$D \rightleftharpoons D^+ + e^-$$

For instance, the presence of 1 at. % of doping agent represents ca 3×10^{20} e^-/cm^3, which is much higher than the instantaneous concentration of photoelectrons created. Therefore, the recombination rate R becomes

$$R = k_R[e^-][h^+] \simeq k_R \times 3 \times 10^{20} \times [h^+] = k'_R[h^+] \quad (31)$$

It is several orders of magnitudes larger than that of undoped samples and consequently kills the photocatalytic activity (31).

p-Type Doping. The dissolution of trivalent cations (Al^{3+}, Ga^{3+}, Fe^{3+}, and especially Cr^{3+}) creates acceptor centers A according to:

$$[(-M^{3+}-)\square] + e^- \rightleftharpoons [(-M^{3+}-)e^-]$$

or

$$A + e^- \rightleftharpoons A^-$$

Filled acceptor centers A^- electrostatically attract holes:

$$A^- + h^+ \longrightarrow A$$

the final mass balance being:

$$e^- + h^+ \longrightarrow N$$

Most of holes h^+ react with A^- and there results a catastrophic behavior with an activity 10^2 times smaller, as demonstrated in Refs. (31,32).

6.3. Reaction of Holes with Oxygen. In equilibrium with oxygen (air), titania chemisorbs two oxygen species, O_2^- and O^-, whose existence has been detected by photoconductivity (30–32). The first species photoadsorbs associatively by trapping one electron:

$$O_2(g) + e^- \longrightarrow O_2^-(ads)$$

The other species photoadsorbs dissociatively

$$1/2\,O_2(g) + e^- \longrightarrow O^-(ads)$$

Subsequently, both adsorbed species react with holes causing their desorption. O_2^- photodesorbs as:

$$O_2^-(\text{ads}) + h^+ \longrightarrow O_2(\text{g})$$

whereas the second species gives an excited, dissociated species

$$O^-(\text{ads}) + h^+ \longrightarrow O^*(\text{ads})$$

which is responsible for photocatalytic mild oxidation reactions, as evidenced by *in situ* photoconductivity measurements performed during photocatalysis (30).

6.4. Reactions of Holes with Water. In water, owing to its amphoteric hydroxyl groups, titania's surface is totally hydrated and hydroxylated. Therefore, the presence of OH^- anions is a source of hole consumption

$$OH^-(\text{ads}) + h^+ \longrightarrow OH^\circ(\text{ads})$$

OH° radicals are known as strong unselective oxidizing agents (actually, the second strongest oxidant behind fluorine). As a consequence, in aqueous media, uv-irradiated titania in the presence of air becomes a strong oxidant, able to destroy almost all organics dissolved, which it comes in contact with.

6.5. Reaction of Holes with Carboxylic Acids (the ''Photo-Kolbe'' Reaction). The direct reaction of holes with carboxylates ions in water was discovered in 1978 (33). It is a very important reaction since it is responsible for the total mineralization of water pollutants with the first loss of a carbon atom:

$$R - COO^- + h^+ \longrightarrow R - COO^\circ \longrightarrow R^\circ + CO_2(\text{g})$$

followed by successive ones linked to the progressive formation of oxidation fragments.

6.6. Reactions of Holes in Reducing Atmospheres. Titania is able to produce hydrogen from alcoholic compounds (biomass) or to catalyze deuterium-alkane isotopic exchange, provided it is associated with a deposited noble metal co-catalyst (17–21). In the case of alcohol dehydrogenation, either in pure organic liquid phase or in aqueous solution, it was shown from kinetics that alcohols adsorbs dissociatively on two different sites, forming an alcoholate anion and a proton:

$$R - CH_2OH \xrightarrow{+TiO_2} R - CH_2O^-(\text{ads}) + H^+(\text{ads})$$

The photo-holes h^+ react selectively with the alcoholate anions giving activated radical which deactivate in giving aldehydic or a ketonic carbonylated molecules plus a hydrogen atom which recombines in di-dihydrogen at the surface of the metal

$$R - CH_2O^- + h^+ \longrightarrow R - CH_2O^\circ$$
$$R - CH_2O^\circ \longrightarrow R - CHO + H^\circ$$
$$2\,H^\circ \longrightarrow H_2(\text{g})$$

In the deuterium-alkane isotopic exchange (DAIE), all the initial OH^- surface groups are spontaneously deuterated by D_2-spillover from the metal onto the surface of titania. The photoholes neutralize OD^- species, forming an activated OD° radical able to exchange one H atom from the C-H bonds of the alkanes:

$$OD^- + h^+ \longrightarrow OD^\circ$$
$$OD^\circ + R - H \longrightarrow R - D + H^\circ$$

The light hydrogen atoms are subsequently removed as HD molecules into the gas phase via the surface atoms of the metal at the M-TiO_2 interface (20,21).

7. Types of Photocatalytic Reactions

According to the section 6, the precious species are the minority charge carriers, ie, the holes, whose reactions with donor molecules or species condition the overall nature of the reaction.

7.1. Oxidation Reactions. For these reactions, two opposite behaviors can be accounted according to the presence of water. This summarized in Table 1.

Selective Mild Oxidation Reactions. The gas phase oxidations using air as the oxidizing agent mainly concerned the mild oxidation of alkanes, alkenes and alcohols into carbonyl-containing molecules (aldehydes and ketones) (32). Inorganics could be also oxidized: CO into CO_2 and NH_3 into mainly nitrogen (80%) (34). NO could be photocatalytically decomposed into N_2 at low pressures and into N_2O at higher pressures, whereas the oxygen generated could be used as an oxidizing agent for butanols (35).

Liquid phase reactions concerned the selective mild oxidation of liquid hydrocarbons (alkanes, alkenes, cycloalkanes, aromatics) into aldehydes and ketons (36). For instance, cyclohexane and decaline were oxidized into cyclohexanone and 2-decalone, respectively with an identical selectivity (86%) (37). Aromatic hydrocarbons (38) such as alkyltoluenes or o-xylenes were 100% selectively oxidized on the methyl group into alkylbenzaldehyde.

Pure liquid alcohols were also oxidized into their corresponding aldehydes or ketones. In particular, the oxidation of isopropanol into acetone was chosen as a photocatalytic test for measuring the efficiency of passivation of TiO_2-or ZnO-based pigments in paintings against weathering.

The high selectivity was ascribed to a photoactive neutral, atomic oxygen species

$$O^-_{(ads)} + h^+ \longrightarrow O^*_{(ads)}$$

These reactions can constitute an environmental friendly ensemble of solutions in fine chemistry as illustrated in the following.

Case Study of the Oxidation of 4-tertio-butyltoluene. The selective oxidation of 4-*tertio*-butyl-toluene in 4-*tertio*-butyl benzaldehyde constitutes an important intermediate reactions in fine chemistry, especially in perfume industry. It is a non catalytic reaction but a stroichiometric one, using permanganate in

a strongly acidic medium according to the equation:

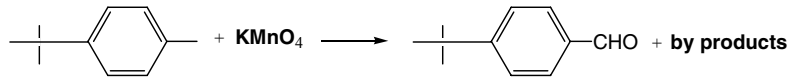

$$5\,C_4H_9-C_6H_4-CH_3+4\,KMnO_4+6\,H_2SO_4\longrightarrow$$
$$4\,MnSO_4+2\,K_2SO_4+11\,H_2O+5\,C_4H_9-C_6H_4-CHO$$

In the final products, there results a lot of inorganic salts, plus an excess of sulfuric acid and many organic by products.

By contrast, either in gas phase or better in pure liquid phase, the photocatalytic mild oxidation, using only uv-irradiated titania plus air, gives 100% selectivity in 4-*tertio*-butyl-benzaldehyde:

$$C_4H_9-C_6H_4-CH_3+O_2(\text{air})\xrightarrow{TiO_2+h\nu}C_4H_9-C_6H_4-CHO+H_2O$$

This is a typically example of "Green Chemistry" which strongly respects the Environmental Factor "E" first described by Sheldon.

Photocatalytic Reactions Involving Hydrogen. In photocatalytic reactions involving hydrogen, either as a reactant [deuterium-alkane isotopic exchange (19)] or as a product (alcohol dehydrogenation (17,18), the system requires the presence of a metal acting as a co-catalyst necessary to dissociate the reactant (D_2) and to recombine H and D into dihydrogen (or HD). Additionally, the metal attracts electrons by photoinduced metal-support interaction (PMSI), decreases the electron-hole recombination and makes the reaction run catalytically (21).

Total Oxidation Reactions in Presence of Water. The selective mild oxidation reaction could be obtained in gaseous or liquid organic phases. By contrast, as soon as water is present, the selectivity turns in favor of total oxidative degradation. This was ascribed to the photogeneration of stronger, unselective, oxidizing species, namely OH° radicals originating from water via the OH^- groups of titania's surface:

$$(H_2O\rightleftharpoons H^+ + OH^-)_{ads}+p^+\longrightarrow H^+ + OH^\circ$$

$\text{Reactant}+OH^\circ\rightarrow\text{Intermediates}\rightarrow\text{Final}$ inorganic products (CO_2, H_2O, H^+, X^-, A^-, etc)

OH° radicals are known as the second best oxidizing agent after fluorine.

Consequently, this system is the most promising issue for an application of heterogeneous photocatalysis, since it is directly connected to water detoxification and to pollutant removal in aqueous effluents.

8. Photocatalytic Water Decontamination

Besides the main field of organic pollutant removal, photocatalysis can efficiently operate in water decontamination either by detoxifying inorganic pollutants or recovering heavy metals.

8.1. Inorganic Pollutants. *Inorganic Anions.* Various toxic anions can be oxidized into harmless or less toxic compounds by using TiO_2 as a photocatalyst. For instance, nitrite is oxidized into nitrate (39), sulfide, sulfite (33) and thiosulfate (40) are converted into sulfate, whereas cyanide is converted either into isocyanide (41) or nitrogen (42) or nitrate (43). Generally, the central element (S,N,P,C, etc) is converted at its maximum oxidation state. These reactions are presented in Fig. 5.

Noble Metal Recovery. Heavy metals are generally toxic for human beings since they accumulate in the body. They can be removed from industrial waste effluents (40,44–47) as small crystallites deposited on the photocatalyst according to:

$$M^{n+} + H_2O \xrightarrow[\text{semiconductor}]{h\nu} > M^{\circ} + nH^{+} + \frac{n}{4}O_2$$

provided the redox potential of the cation metal couple is higher than the flat band potential of the semiconductor.

Under identical conditions, the following photodeposition reactivity pattern was found:

$$Ag > Pd > Au > Pt \gg Rh \gg Ir \gg Cu = Ni = Fe = 0$$

using the following inorganics as reactants: $AgNO_3$, $PdCl_2$, $AuCl_3$, H_2PtCl_6, or Na_2PtCl_6, $RhCl_3$, H_2IrCl_6, $Cu(NO_3)_2$, $Ni(NO_3)_2$, and $Fe(NO_3)_3$.

Note that this method can also be used to prepare noble metal catalysts promptly deposited (~10 minutes) in a single step, at room temperature and in mild "Chimie Douce" conditions on photosensitive oxide supports (48–52).

In view of the above relative activity pattern, most of the experiments were carried out with platinum and silver, using TiO_2 as the photocatalyst. The deposition initially occurred by forming small homodispersed crystallites whose size depended on the nature of the metal: 0.8–1 nm for Ir, 1–1.5 nm for Pt (51) and ca. 3 nm for Ag (40). As the photodeposition conversion increases, the metal particles form agglomerates, reaching several hundreds of nm (ie, bigger than the TiO_2 particles) themselves for Ag (40). Since these agglomerates contained the major part of the metal deposited, the photosensitive surface was not markedly masked and high amounts of metals were recovered. The final concentrations of easily photoreduced cations are lower than the detection limits of atomic absorption spectroscopy (≤ 0.01 ppm). Silver photodeposition has been applied with two environmental interests: (*1*) the recovery of Ag from used photographic baths in which the silver-thiosulfate complex is decomposed, Ag^+ is reduced to Ag° and (*2*) the detoxification of the aqueous effluent, $S_2O_3^{2-}$ oxidized into SO_4^{2-} (40), whereas phenolic compounds are degraded into CO_2 (53).

Because of their favorable redox potentials, only noble metals can be photodeposited. This property has been used to selectively recover heavy noble metals. For instance, silver was separated from copper in solutions simulating industrial electrolytic baths. Other toxic, heavy, non-noble metals could be removed from water. Mercury, because of its favorable redox potential, was photoreduced as zerovalent metal (54). The cations Pb^{2+} and Tl^{+} were deposited on uv-irradiated TiO_2 powder as PbO_2 and Ti_2O_3 (55). Similarly, uranium was photodeposited on TiO_2 as U_3O_8 from uranyl solutions (56).

From an application point of view, the recovery of silver from photographic baths seems the most promising issue, provided the legislation towards Ag-containing discharge water becomes more strict.

8.2. Organic Pollutants. The aim of the studies presented here was to establish correlations between the molecular structure of the pollutants and their photocatalytic degradability. The analyses of the various intermediates were carried out both to have an idea of the degradation pathways and to determine whether toxic and stable compounds are generated. An illustrative list of aqueous organic pollutants which can be mineralized in innocuous products is given Table 2.

Disappearance of the Pollutant. The dearomatization is rapid even in the case of deactivating substituents on the aromatic ring. This was observed for the following substituents: Cl (33,57,58), NO_2 (59), $CONH_2$ (60), CO_2H (33) and OCH_3 (61). If an aliphatic chain is bound to the aromatic ring, the breaking of the bond is easy as was observed in the photocatalytic decomposition of herbicide 2,4-D (2,4-dichlorophenoxyacetic acid) (62,63) and tetrachlorvinphos ((*Z*)-2-chloro-1 (2,4,5-trichlorophenyl) ethenyl dimethyl phosphate) (64), and phenitrothion (65).

Total Mineralization of Organic Pollutants. The oxidation of carbon atoms into CO_2 is relatively easy. It is, however, in general markedly slower than the dearomatization of the molecule. Until now, the absence of total mineralization has been observed only in the case of *s*-triazines herbicides, for which the final product obtained was essentially 1,3,5-triazine-2,4,6, trihydroxy (cyanuric acid) (66), which is, fortunately, not toxic. This is due to the high stability of the triazinearomatic ring, which resists most oxidation methods. For chlorinated molecules, Cl^{-} ions are easily released in the solution (33,57,58) and this could be of interest in a process, where photocatalysis would be associated with a biological epuration system which is generally not efficient for chlorinated compounds. Nitrogen-containing molecules are mineralized into NH_4^{+} and mostly NO_3^{-} (60). Ammonium ions are relatively stable and the proportion depends mainly on the initial oxidation degree of nitrogen and on the irradiation time (67). Actually, NH_4^{+} ions are photodegradable provided an alkaline pH since at acidic pH, the surface of titania is positively charged and repels cations (68).

The pollutants containing sulfur atoms are mineralized into sulfate ions (65,67). Organophosphorous pesticides produce phosphate ions (64,65,69,70). However, phosphate ions in the pH range used remained adsorbed on TiO_2. This strong adsorption partially inhibits the reaction rate which, however, remains acceptable (64,65,71). Until now, the analyses of aliphatic fragments resulting from the degradation of the aromatic ring have only revealed formate and acetate ions. Other aliphatics (presumably acids, diacids, hydroxylated

compounds) are very difficult to separate from water and to analyze. Formate and acetate ions are rather stable, as observed in other advanced oxidation processes, which in part explain why the total mineralization is much longer that the dearomatization reaction.

Degradation Pathways: Case Study of Pesticides. Primary intermediates detected and identified by hplc, lc/ms and gc/ms of the photocatalytic degradation of various aromatic pollutants correspond to the hydroxylation of the benzene ring. These intermediates have very low transient maximum concentrations with respect to that of the initial pollutant in agreement with the fact that CO_2, acetate and formate are formed in the initial stages of the degradation. The orientation of the hydroxylation of the aromatic ring depends on the nature of the substituents. For instance, for chlorophenols and dimethoxybenzenes, the para and ortho positions (with respect to OH for the chlorophenols) are favored as expected.

The degradation pathways are illustrated here by the examples of fenitrothion (Fig. 6).

Fenitrothion has the following formula:

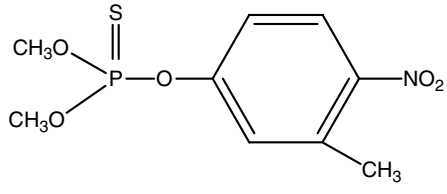

This organo-thio-phosphorus is very dangerous since it first oxidizes into fenitrooxon,

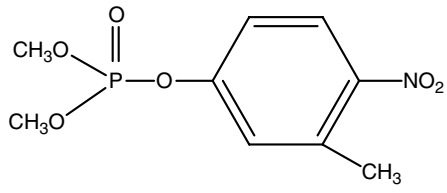

which can be found in warfare gases. Fortunately, this first toxic intermediate is easily degraded, as its subsequent metabolites, into final innocuous inorganic products as demonstrated by the mass balance analysis, according to the overall equation:

$$(CH_3O)_2 - P(S) - O - C_6H_3 - (NO_2)(CH_3) + \frac{13}{2}O_2 \longrightarrow$$
$$9\,CO_2 + 3\,H_2O + 4\,H^+ + H_2PO_4 + SO_4^{2-} + NO_3^-$$

This particular efficiency of titania has been utilized for producing efficient gas masks for the U.S. army in contaminated areas (68). The air purification follows the same reaction mechanism, provided a minimum humidity in air to maintain an hydrated state of titania's surface, source of the hydroxyl groups, precursors

of OH° radicals. In addition, this surface hydration is easily maintained by the formation of water during oxidation of the C-H bonds of organic pollutants to be destroyed. Such air purification has been recently successfully applied to the removal of odors in confined atmospheres, as for instance in domestic refrigerators (72).

Organic Pollutant Removal: Case Study of Azo Dyes. The organic pollutant removal is the main application of water photocatalytic decontamination. Most of aliphatic and aromatic pollutants are totally mineralized into CO_2 and innocuous inorganic anions (Cl^-, SO_4^{2-}, NO_3^-). More complex molecules such as pesticides (herbicides, insecticides, fungicides etc) or dyes are also totally destroyed. Presently, concerning dyes worldwide used, half of them are azo-dyes (ie, containing the $-N{=}N-$ azo group). Several examples, Cibacron Brilliant Red 3B-A, Remazol Black B (Reactive Black 5), Congo Red (73), Methyl Red (73), Orange G (73), Amaranth (74), Orange Yellow and Patented Blue, were all successfully destroyed and totally mineralized. The developed formula is given for two of them: Congo Red, which is an industrial dye particularly recalcitrant for decolorization and Amaranth which is a prohibited carcinogenic alimentary dye (Fig. 7). The stoichiometric coefficients of the total degradation, as well as the mass balances, were established for different elements (carbon, hydrogen, oxygen, sulfur), but not for nitrogen (nitrogen mass balance established in the aqueous solution based on nitrate and ammonium ions). Using an air-tight batch slurry photoreactor connected to an air-tight gas chromatograph an evolution of N_2 in the gas phase could be evidenced and quantified. For example, N_2 evolution from a Congo Red solution is given Fig. 8. The kinetics curve reached a plateau at $t_{UV} = 400$ min (Fig. 8) and the total mass balance in nitrogen was found equal to 100 %. In addition, the ratio $2n_{N_2}/(n_{NH_4} + n_{NO_3} + 2n_{N_2})$ was found equal to 0.65, ie, just corresponding to the ratio 2/3 of the number of N atoms contained in the double $-N{=}N-$ azo-groups to the total number of N contained in Congo Red. Similar results for all the other azo-dyes mentioned above. This means that photocatalytic degradation of azo-compounds is 100% selective in generating gaseous dinitrogen.

This is the first example –to the author's knowledge- of a nitrogen evolution during the aqueous photocatalytic degradation of complex N-containing pollutants. This constitutes an ideal example of water decontamination.

9. Tentative Modifications of the Catalysts

9.1. Noble Metal Deposit. *Reactions Involving Hydrogen.* In photocatalytic reactions involving hydrogen (or deuterium), either as a reactant (deuterium-alkane isotopic exchange or as a product (alcohol dehydrogenation (17,18)), the system requires the presence of a metal acting as a co-catalyst necessary to dissociate the reactant (D_2) and to recombine H and D into dihydrogen (or HD). Additionally, the metal attracts electrons, by photoinduced metal-support interaction (PMSI), decreases the electron-hole recombination, and maintains the turn-over number constant (21).

Oxidation Reactions. The same catalysts based on Pt deposited on titania were also used in oxidation reactions. However, the beneficial effects observed for

hydrogen-involving reactions became detrimental for total oxidation reactions. This was accounted for by the electron transfer to metal nanocrystallites which became concurrent to dioxygen ionosorption.

$$\mathrm{Pt} + e^- \rightleftharpoons e^-_{(\mathrm{Pt})}$$
$$\mathrm{O_2(g)} + e^- \rightleftharpoons \mathrm{O^-_{2(ads)}}$$

In addition, once negatively charged, platinum particles became attractive for holes which recombined with electrons into neutral centers (eq. 17) with production of inefficient thermal energy. Since deposited metals act as recombination centers in oxidation reactions, efficient photocatalysts should not contain noble metals, which is of a great advantage for (solar) cheap photocatalytic applications.

9.2. Ion Doping. Another modification was aimed at extending the photosensitivity of titania to the visible region to harvest cheaper and more abundant solar efficient photons. The best expected case would have been Cr^{3+}-doping, since its absorption spectrum gives an important shoulder in the visible.

Unfortunately, Cr^{3+}-doping was found to strongly inhibit photocatalysis and decrease the quantum yield (75,76). This detrimental behavior was confirmed by ion doping, either of the n-type (by dissolving pentavalent heterocations such as Nb^{5+}, Sb^{5+}, Mo^{6+}, Ta^{5+} in the lattice of titania) or of the p-type (by dissolving trivalent heterocations such as Ga^{3+}, Al^{3+}). This was explained by the fact that both pentavalent donor impurities and trivalent acceptor impurities behave as electron-hole recombination centers. However, this drawback could be turned into advantage by using ion doping as a means of passivating TiO_2-based pigments in paintings and plastics against weathering (77).

10. Polyphasic (Solar) Photoreactors

To perform the various types of photocatalytic reactions described above, different types of photoreactors have been built with the catalyst used in various shapes: fixed bed; magnetically or mechanically agitated slurries; catalyst particles anchored on the walls of the photoreactor; or in membranes or on glass beads; or on glass-wool sleeves, small spherical pellets, etc (1–4). The main purpose is to have an easy separation of the catalyst from the fluid medium, thence the necessity to support titania and to avoid the final ultrafine particle filtration.

Various devices have been developed such as TiO_2-coated tubular photoreactors, annular and spiral photoreactors, falling-film photoreactors. Initially, two systems were commercialized by Matrix Photocatalytic, Inc., of Ontario, Canada and Purifies Environmental Technologies, Inc., London, Ontario, Canada. One uses powder TiO_2 and concerns the market of wastewater treatment. In the other system, TiO_2 is supported on a fiber glass mesh cloth in which a cylindrical uv lamp is wrapped.

An evaluation of ultraviolet oxidation methods was carried out for the removal of 2, 4, 6-trinitrotoluene from groundwater (78). These methods were

TiO_2/UV, O_3/UV, H_2O_2 + additive/UV. Heterogeneous photocatalysis was found to be the most economical. Even though several criticisms can be made to this evaluation, it comes out that heterogeneous photocatalysis appears as a method that can compete economically with other UV oxidation processes for water treatment.

The most effective photocatalysts are anatase samples which absorb only ca. 3 % of the overall solar energy at the earth's surface. In spite of that, large-scale tests have been built or modified and are still used in North-America, Israel and Europe (Plataforma Solar de Almeria (PSA), Spain) (see also Ref. 78) to collect data in order to estimate the cost of water treatment. Solar reactors that do not concentrate the incident light have lower hardware cost, eliminate photon losses at reflecting surfaces and use diffused sunlight (78–87). For these non concentrating systems, estimates have concluded that solar photons can be used at a lower cost than photons from uv lamps (78). Solar photocatalysis has been baptized "Heliophotocatalysis" by the author. One could have denoted it heliocatalysis, but it is not accurate enough since one could have a heliothermocatalysis, which would use the concentrated ir beams of the sun. That is not yet under study.

10.1. Case Study of the Compound Parabolic Collector (CPC) Photoreactor at PSA. The principle of the CPC photoreactor used at Plataforma Solar de Almeria (PSA) in Spain is described in the scheme of Fig. 9A, whereas the collector itself is described in Fig. 9B with an inclination angle of 37° corresponding to the latitude of Almeria. The CPC collector which is the irradiated part of the system corresponds to a plug flow reactor but, since it is connected to a tank via a recirculation pump, the ensemble corresponds to a batch reactor. Since the elimination of pesticides follows a first-order kinetics (see section 4.3.), the concentration C_{Ao} at the inlet and C_A at the outlet of the collector are related by the equation

$$C_A/C_{Ao} = \exp(-kt) \tag{32}$$

Because of the recirculation, C_{Ao} varies with time as:

$$-V_2(dC_{Ao}/dt) = Q(C_{Ao} - C_A) \tag{33}$$

where V_2 is the volume of the tank, and Q is the flow rate. Combining eqs. 32 and 33, one gets:

$$-V_2(dC_{Ao}/dt) = Q[C_{Ao} - C_{Ao}\exp(-kV_1/Q)] = QC_{Ao}[1 - \exp(kV_1/Q)] \tag{34}$$

where V_1 is the volume of the irradiated part of the reactor.

The integration of differential equation (34) gives:

$$[CAo]_{final} = (CAo)_{initial} \exp[-(1 - \exp(-kV_1/Q)][Q \cdot t/V_2] \tag{35}$$

If the flow rate Q is high and if V_1 is not too important, eq. (35) can be simplified

$$\exp(-kV_1/Q) = \exp(-\varepsilon) \approx 1 - \varepsilon = -kV_1/Q$$

$$\text{Thence}[C_{Ao}] = [C_{Ao}]_{\text{initial}} \exp[(-kV_1/Q) \times (Q/V_2)t] \quad (36)$$

$$= [C_{Ao}]_{\text{initial}} \exp(-k(V_1/V_2)t) \quad (37)$$

The residence time t_R in the CPC collector is equal to

$$t_R = [V_1/V_T]t = [V_1/(V_1 + V_2)]t = [r/(1 + r)]t \quad \text{with} \quad r = V_1/V_2 \quad (38)$$

Therefore eq. (37) becomes:

$$C_{Ao} = [C_{Ao}]_{\text{initial}} \exp[-(1 + r)/r)kt_R] \quad (39)$$

By determining ratio r from the geometry of the reactor, one can calculate the apparent first-order reaction rate constant, k.

The solar photocatalytic degradation of pollutants in the CPC photoreactor has been successfully applied at PSA on various pollutants (15,63,79–87). These experiments can be examplified by the total mineralization of 2,4-D (2,4 -dichlorophenoxyacetic acid) (62,63), a well known herbicide. In Fig. 10 are represented the temporal variations of 2,4-D, of 2,4-dichlorophenol (2,4-DCP) the main intermediate formed, of Cl^- anions produced and of the total organic carbon (TOC). After an adsorption period of 1 h in the dark, 2,4-D disappears following a first order kenetics. Cl^- anions follow a sigma shaped curve in agreement with the consecutive reaction scheme:

$$2,4 - \text{D} \xrightarrow{k_1} 4 - \text{DCP} \xrightarrow{k_2} 2\,\text{Cl}^- + 8\,\text{CO}_2 \quad (40)$$

giving

$$[\text{Cl}^-] = 2\,\text{C}_\text{O}[1 - k_2/(k_2 - k_1)\exp(-k_1t) + k_1/(k_2 - k_1)\exp(-k_2t)] \quad (41)$$

The TOC decreases linearly to zero within 1 h with an apparent zero kinetic order. That could be interpreted by assuming a saturation of surface sites by all the intermediates.

$$-d[TOC]/dt = +d[\text{CO}_2/dt = k\Sigma\theta_i = k\Sigma K_iC_i/(1 + K_iC_i) \approx k\theta_{sat} \approx k \quad (42)$$

where θ_i represents the surface coverage of the i^{th} intermediate and θ_{sat} is the overall coverage at saturation. It can be seen in Table 3 that both rate constants of 2,4 D and of TOC disappearance are quite proportional to the mean solar uv power flux, which can vary with the weather. This means, according to Fig. 4, that the CPC is working in optimal conditions with respect to solar irradiation and can also work with diffuse uv-light.

These experiments were compared with initial studies performed in a laboratory microphotoreactor working with artificial light, which is described

in Fig. 3. Despite a volume extrapolation factor of 12500, the same first order was found for 2,4-D disappearance; the intermediates were the same, indicating an identical reaction pathway; the quantum yields were the same. Only two points of apparent divergence were observed: (*1*) the optimum concentration in titania for the CPC pilot plant was 0.2 g/L instead of 2.5 g/L for the batch microreactor; and (*2*) the TOC disappearance at PSA was faster than the CO_2 evolution in laboratory experiments. This was ascribed to the CPC photoreactor design (63) with a recirculating tank which favors the production of the final products detrimentally to that of the intermediate ones (88).

The photocatalytic degradation at PSA is applied to the treatment of used waters contaminated by a large variety of pesticides after the washing of shredded empty herbicide containers (about 1.5 million collected per year), in a plant built for the decontamination and the recycling of plastic. Indeed, herbicides are intensively used in the province of Almeria, which has become an important producer of fruit and vegetables in green houses because of the very sunny climate. If the demonstration of the technical and economical feasibility of the process is achieved, the city of El Ejido, located in the center of the greenhouse area, will become the first European town to include a solar photocatalytic plant in a real waste treatment process.

10.2. Solar Photocatalytic Reactor using Deposited Titania. Although slurry photoreactors can be estimated as the most efficient, they exhibit an important drawback: the final tedious filtration of titania particles. To overcome this obstacle, titania can be deposited on photoinert supports. A successful attempt was obtained by depositing titania on a special Ahlstrom paper using amorphous silica as a binder to anchor the photocatalyst particles on inorganic fibers (92). Such photocatalytic material has been used in an adapted solar photoreactor called Cascade Falling Films Photoreactors (CFFP) described in Figs. 11 and 12.

The photocatalytic activity is based on the rate of the total organic carbon (TOC) removal from a solution containing 50 ppm of 4-chlorophenol chosen as a model pollutant.

To test the efficiency of CFFP solar reactor, photocatalytic reactions were calibrated against a slurry CPC photoreactor having the same surface of sun collector as shown on photographs in Fig. 12. Surprisingly, the results were similar in the total degradation of 4- chlrorophenol as indicated by the TOC disappearance (Fig. 12).

These fixed bed photoreactors are presently under study to produce drinking water for remote isolated human communities in arid countries (North Africa: the European AQUACAT Program (90); Latin America: The European SOLWATER Program (91).

Besides fixation of titania on a support, a material science is being developed for the preparation of thin layers of titania on “self-cleaning” objects such as glasses, concrete walls, ceramics, tools etc.

11. Natural Photocatalytic Processes in the Environment

11.1. Natural Photocatalytic Reactions in the Atmosphere. Urban atmosphere contains pollutants and solid particles. Some of them originate from soils such as silicoaluminates and Fe_2O_3 and others such as TiO_2 from anthropogenic activities (fly ashes) (92). These aerosols are able to chemisorb atmospheric pollutants and to be photoactivated by sun light during day time. Orthoxylene (93) and naphthalene (94) were chosen as model atmospheric pollutants. In dry conditions, illuminated titania oxidizes *o*-xylene into *o*-tolualdehyde in agreement with the oxidative properties of titania (38). By contrast, in the presence of water which is a constituent of the atmosphere, the oxidation becomes total with the formation of CO_2 and H_2O, because of the photoinduced generation of OH° radicals (see section 6.4).

11.2. Natural Photocatalytic Reactions on Sands. Crude-oil residue in contact with beach sand and air has been observed to undergo photocatalytic oxidation on exposure to light (95). The beach sand used contained magnetite and ilmenite as minor constituents. These materials are known to have catalytic properties for hydrocarbon oxidation. These results indicate examples of environmental photoassisted "self-cleaning" processes.

11.3. Geophotocatalysis: Photocatalytic Origin of the Varnish of Rocks. Solar photocatalytic processes can be responsible for the color of a landscape. For instance, most parts of Sahara, mountains are dark brown, whereas sand is yellow. Flat stones laying on the ground are in the shape of slabs. Their upper faces exposed to sun are dark brown, whereas their lower faces in contact with the soil are yellow. EDX analyses revealed that the dark color was mainly constituted by manganese oxides (96,97). Titanium ions (ie, titania) were permanently found when MnOx was present (95,96). A possible photocatalytic oxidation of Mn^{2+} ions by traces of titania can be proposed to account, at least partially, for this oxide formation at the solar light exposed surfaces of the rocks and stones.

11.4. Self-Cleaning Objects. Finally, solar photocatalysis is the actually efficient process, which makes self-cleaning glasses work (98–101). Fouling of glasses is mainly due to dust and/or atmospheric particles stuck at the surface on greasy stains mainly constituted of fatty acids. Self-cleaning glasses are coated with an invisible thin layer of titania, which under the simultaneous presence of oxygen (air), atmospheric water vapor and solar uv-light, is able to decompose fatty acids by successive photodecarboxylations ["photo-Kolbe", (41)] reactions and let coated glasses recover their initial clarity.

12. Present Challenges in Photocatalysis

After the pioneer work described in this article, photocatalysis reached its maturity as a new discipline in the field of catalysis. In the future, it will have to address the following challenges:

1. Are we limited to work exclusively with titania?

The author estimates that the answer is "yes". Why? As mentioned at the beginning of this chapter, the best photocatalyst must combine excellent photon **AB**sorption and excellent reactant **AD**sorption. Up to now, only titania fulfils both requirements.

2. Can TiO_2 be photosensitized in the visible by doping?

   Years ago (31), the author demonstrated that photosensitizing titania in the visible by cationic doping was not only inefficient but also strongly detrimental. Presently, it is tried elegantly to reduce the energy band gap of titania by elevating its valence band via anionic doping. This is really a new concept. Anionic doping is based on the dissolution of hetero-anions such as N^{3-}, S^{2-}, which creates an acceptor energy band in the band gap of titania. Definitive probant results are still being waited for at the moment. The difficulty is to preserve the integrity of the dissolved hetero-anion. N^{3-} and S^{2-} anions are submitted to the strong oxidizing power of titania. Some information indicate that the stability of these foreign species in lattice positions is not obtained up to now. Therefore, anionic doping constitutes a real present challenge.

3. Can we find a new photocatalyst different from TiO_2 and directly active in the visible?

   This is a hard challenge since such a miraculous catalyst has not been yet found. As repeated above, it will have to simultaneous combine a good **AD**sorption capacity and a good **AB**sorption of visible photons, as well as titania does in the near-uv range.

4. Is photocatalysis suitable for preparative fine chemistry?

   The author estimates that this is the easiest challenge among those proposed. It is illustrated in section 7.1.2 and corresponds to fine chemistry applications. The advantage is the high initial selectivities obtained in mild oxidation reactions. However, it implies a strong development in the photocatalytic engineering.

5. Is photocatalysis enough bactericide in water and in air?

   This challenge must be addressed. Actually, water treatment requires not only detoxification by eliminating or "neutralizing" harmful chemical pollutants but also disinfection by killing and degrading bacteria and viruses dangerous for human health.

6. Is photocatalysis really $\ll$ cancericide $\gg$?

   This is a typical interdisciplinary challenge between chemistry and medicine. This path was opened a few years ago by Fujishima and co-workers (102) and potentialities should be explored more deeply.

7. Are we able to define a few standardized tests for any photocatalytic system?

   This problem is really a present one since photocatalytic activities or efficiencies for different systems produced and commercialized should refer to official standards for a true estimation of their performances. Some tests, such as dye decolorization, are not suitable for a real estimation of the activities of photocatalysts since spontaneous photochemical side reactions occur and perturb or even mask the real activity of the solids.

13. Conclusions

An overview has been presented on the various aspects and potentials of heterogeneous photocatalysis. The potential applications strongly depend on the future development of the photocatalytic engineering.

Water pollutant removal appears as the most promising potential application since many toxic water pollutants, either organic or inorganic are totally mineralized or oxidized at their higher degree, respectively, into harmless final compounds. Besides some drawbacks (use of uv-photons and necessity for the treated waters to be transparent in this spectral region; slow complete mineralization in cases where heteroatoms are at a very low oxidation degree; photocatalytic engineering to be developed), room-temperature heterogeneous photocatalysis offers the following interesting advantages (5): chemical stability of TiO_2 in aqueous media and in large range of pH ($0 \leq pH \leq 14$); low cost of titania (ca.16€/kg); cheap chemicals in use; no additives required (only oxygen from the air); system applicable at low concentrations; great deposition capacity for noble metal recovery; absence of inhibition or low inhibition by ions generally present in water; total mineralization achieved for many organic pollutants; efficiency of photocatalysis with halogenated compounds sometimes very toxic for bacteria in biological water treatment; and possible combination with other decontamination methods (in particular biological).

Heterogeneous photocatalysis is now reaching the preindustrial level. Several pilots and prototypes have been built in various countries. However, one has to be realistic. Because of the quantum yield and of the incident efficient photon flux, photocatalysis is necessarily devoted to limited devices. More precisely, this means that a reasonable size photoreactor would be able to treat from 1 to a few tens of m^3 of aqueous effluents / day.

In parallel, photocatalysis can be applied to air treatment provided the presence of a minimum humidity to favor the formation of OH° radicals detrimentally to that of dissociated activated oxygen O* species responsible for selective mild oxidation reactions as developed in Ref. 9.

14. Acknowledgments

The author thanks CNRS and European Community (Programs AQUACAT and SOLWATER) for financial support. He is also indebted to Mrs Christine Delbecque for her valuable help in preparing the manuscript.

BIBLIOGRAPHY

"Photochemical Technology" in *ECT* 2nd ed., Vol. 15, pp. 331–354, by C. R. Mullen, The Dow Chemical Co.; in *ECT* 3rd ed., Vol. 17, pp. 540–559, by J.J. Bloomfield and D.C. Owsley, Monsanto Co.; "Photocatalysis" under "Photochemical Technology" in *ECT* 4th ed., Vol. 18, pp. 820–837, by Nick Serpone, Concordia University; "Photocatalysis" in *ECT* (online), posting date: December 4, 2000, by Nick Serpone, Concordia University.

CITED PUBLICATIONS

1. M. Schiavello ed., *Photocatalysis and Environment*, Kluwer Academic Publishers, Dordrecht, 1988.
2. N. Serpone and E. Pelizzetti eds., *Photocatalysis, Fundamentals and Applications*, Wiley, New York, 1989.
3. D. F. Ollis and H. Al-Ekabi eds., *Photocatalytic Purification and Treatment of Water and Air*, Elsevier, Amsterdam, 1993.
4. O. Legrini, E. Oliveros, and A. Braun, *Chem. Rev.* **93**, 671 (1993).
5. J. M. Herrmann, *Catal. Today*, **17**, 7 (1999).
6. D. W. Bahnemann and co-workers, in: R. G. Zepp, G. R. Helz, and D. G. Crosby, eds., *Aquatic Surface Photochemistry*, F. L. Lewis Publishers, Boca Raton, 1994, p. 261.
7. R. W. Matthews, *J. Chem. Soc., Faraday Trans. 1*, **80**, 457 (1984).
8. J. M. Herrmann, Chapter 9: *"Water Treatment by Heterogeneous Photocatalysis"* in F. Jansen and R. A. van Santen, eds., Environmental Catalysis, Imperial College Press (London), Catalytic Science Series, 1999, p. 171.
9. J. M. Herrmann, *Helv. Chim. Acta*, **84**, 2731 (2001).
10. M. Kaneko and I. Okura, eds., *Photocatalysis Science and Technology*, Kodanska Springer, 2002.
11. D. M. Blake, *Bibliography of Work on Photocatalytic Removal of Hazardous Compounds from Water and Air*, NREL/TP-430-22197, National Renewable Energy Laboratory, Golden, 1999 and 2001.
12. H. Gerisher, in D. F. Ollis and H. Al-Ekabi eds., *Photocatalytic Purification and Treatment of Water and Air*, Ref. 2, Elsevier, Amsterdam, 1993, p. 1.
13. F. Juillet, F. Lecomte, H. Mozzanega, S. J. Teichner, A. Thévenet, and P. Vergnon, *Faraday Discussion, Symp. Chem. Soc*, **7**, 57 (1973).
14. S. Malato, PhD Dissertation, Almeria University, Spain, 1997.
15. S. Malato Rodriguez, in "Solar Photocatalytic Decomposition of Pentachlorophenol Dissolved on Water; Coleccion Documentos CIEMAT Madrid, 1999.
16. S. Malato Rodriguez, J. Blanco Galvez, and J. M. Herrmann, Guest Editors in: "Solar Catalysis for Water Decontamination", Catal. Today (Special Issue), (2–3) 54 (1999).
17. P. Pichat, J. M. Herrmann, J. Disdier, H. Courbon, and M. N. Mozzanega, *Nouv. J. Chim.* **5**, 27 (1981).
18. J. M. Herrmann, J. Disdier, P. Pichat, *Nouv. J. Chim.* **6**, 53 (1982).
19. H. Tahiri, Y. Aït Ichou, and J. M. Herrmann; *J. Photochem, Photobiol. A: General*, **114**, 219 (1998).
20. H. Courbon, J. M. Herrmann, and P. Pichat, *J. Catal.*, **95**, 539 (1985).
21. J. M. Herrmann, in R. T. K. Baker, S. J. Tauster, and J. A. Dumesic, eds., *Strong Metal-Support Interactions*, Chapt. 20. ACS Symposium Series, **298**, 200 (1986).
22. G. Pass, A. B. Littlewood, and R. L. Burwell Jr., *J. Amer.Chem. Soc.* **82**, 6281 (1960).
23. R. L. Burwell Jr., G. L. Haller, K. C. Taylor, and J.F. Read, in *Advances in Catalysis*, Vol. 20, Academic Press, New York, 1969, p. 1.
24. R. L. Burwell Jr., *Acc. Chem. Res.* **2**, 289 (1969): *Catal.Rev.* **7**, 25 (1972).
25. Y. Inoue, J. M. Herrmann, H. Schmidt, R. L. Burwell Jr., J. B. Butt, and J. B. Cohen, *J. Catal*, **53**, 401 (1978).
26. J. M. Herrmann, M. Gravelle-Rumeau-Mailleau, and P. C. Gravelle, *J. Catal.*, **104**, 136 (1987).
27. P. Pichat and J. M. Herrmann, in Ref. 2.
28. C. Turchi, M. Mehos, and J. Pacheco, in Ref. 3, p. 789.
29. R. Miller and R. Fox, in Ref. 3, p. 573.

30. J. M. Herrmann, J. Disdier, M. N. Mozzanega, and P. Pichat, *J. Catal.*, **60**, 369 (1979).
31. J. M. Herrmann, J. Disdier, P. Pichat, *Chem.Phys. Lett.*, **108**, 618 (1984).
32. J. M. Herrmann, H. Courbon, J. Disdier, M. N. Mozzanega, and P. Pichat, *Stud. Surf. Sci. Catal.*, **59**, 675 (1990).
33. S. N. Frank and A. J. Bard, *J. Phys. Chem.* **81**, 1484 (1977).
34. H. Mozzanega, J. M. Herrmann, and P. Pichat, *J. Phys. Chem.* **83**, 2251 (1979).
35. P. Pichat, J. M. Herrmann, H. Courbon, J. Disdier, and M. N. Mozzanega, *Canad. J. Chem. Eng.* **60**, 27 (1982).
36. W. Mu, J. M. Herrmann, and P. Pichat, *Catal. Lett.* **3**, 73 (1989).
37. J. M. Herrmann, W. Mu, and P. Pichat, *Stud. Surf. Sci. Catal.* **55**, 405 (1990).
38. P. Pichat, J. Disdier, J. M. Herrmann, and P. Vaudano, *Nouv. J. Chim.* **10**, 545 (1986).
39. Y. Hori, A. Nakatsu, and S. Susuki, *Chem. Lett.* 1429 (1985).
40. J.-M. Herrmann, J. Disdier, and P. Pichat, *J. Catal.* **113**, 72 (1988).
41. S. N. Frank and A. J. Bard, *J. Am. Chem. Soc.* **99**, 303 (1977).
42. H. Hidaka, T. Nakamura, A. Ishizaha, M. Tsuchiya, and J. Zhao, *J. Photochem. Photobiol. A: Chem.* **66**, 367 (1992).
43. C. H. Pollema, J. L. Hendrix, E. B. Milosavljevic, L. Solujic, and J. H. Nelson, *J. Photochem. Photobiol. A: Chem.* **66**, 235 (1992).
44. J.-M. Herrmann, J. Disdier, and P. Pichat, *J. Phys. Chem.* **90**, 6028 (1986).
45. E. Borgarello, N. Serpone, G. Eno, R. Harris, E. Pelizzetti, and C. Minero, *Inorg. Chem.* **25**, 4499 (1986).
46. E. Borgarello, R. Harris, and N. Serpone, *Nouv. J. Chim.* **9**, 743 (1985).
47. N. Serpone, E. Borgarello, M. Barbeni, E. Pelizzetti, P. Pichat, J.-M. Herrmann, and M. A. Fox, *J. Photochem.* **36**, 373 (1987).
48. K. H. Stadler and H. P. Boehm in Proc. 8th Inter. Congr. Catal., Dechema, Frankfurt, 1984, vol. IV, p. 803.
49. W. W. Dunn and A. J. Bard, *Nouv. J. Chim.* **5**, 651 (1981).
50. S. Sato, *J. Catal.* **92**, 11 (1985).
51. J.-M. Herrmann, J. Disdier, and P. Pichat, in B. Delmon, P. Grange, P. A. Jacobs and G. Poncelet eds., *Preparation of Catalysts IV*, Elseiver, Amsterdam, 1987, p. 285.
52. J.-M. Herrmann, J. Disdier, P. Pichat, A. Fernandez, A. Gonzalez-Elipe, G. Munuera, and C. Leclercq, *J. Catal.* **132**, 490 (1991).
53. H. Tahiri, N. Serpone, and R. Le van Mao, *J. Photochem. Photobiol. A: Chem.* **93**, 199 (1996).
54. N. Serpone, Y. K. Ah-You, T. P. Tran, R. Harris, E. Pelizzetti, and H. Idaka, *Solar Ener.* **39**, 491 (1987).
55. K. Tanaka, K. Harada, and S. Murata, *Solar Ener.* **36**, 159 (1986).
56. R. Amadelli, A. Maldotti, S. Sostero, and V. Carassitti, *J. Chem. Soc. Faraday Trans.* **87**, 3267 (1991).
57. J. C. D'Oliveira, G. Al-Sayyed, and P. Pichat, *Environ. Sci. Technol.* **24**, 990 (1990).
58. G. Al-Sayyed, J. C. D'Oliveira, and P. Pichat, *J. Photochem. Photobiol., A: Chem.* **58**, 99 (1991).
59. C. Maillard-Dupuy, C. Guillard, and P. Pichat, *New J. Chem.* **18**, 941 (1994).
60. C. Maillard, C. Guillard, and P. Pichat, *New J. Chem.* **16**, 821 (1992).
61. L. Amalric, C. Guillard, N. Serpone, and P. Pichat, *J. Environ. Sci. Health*, **A28**, 1393 (1993).
62. P. Pichat, J. C. D'Oliveira, J. F. Maffre, and D. Mas, p. 683 in Ref. (3) (1993).
63. J. M. Herrmann, J. Disdier, P. Pichat, S. Malato, and J. Blanco, *Appl. Catal. B: Environmental*, **17**, 15 (1998).
64. M. Kerzhentsev, C. Guillard, J. M. Herrmann, and P. Pichat, p. 601, in Ref. (3) 1993.

65. M. Kerzhentsev, C. Guillard, J.-M. Herrmann, and P. Pichat, *Catalysis Today*, **27**, 215 (1996).
66. E. Pelizzetti, V. Maurino, C. Minero, O. Zerbinati, and E. Borgarello, *Chemosphere*, **18**, 1437 (1989).
67. G. K. C. Low, S. R. Mc Evoy, and R. W. Matthews, *Environ. Sci. Technol.* **25**, 460 (1991).
68. M. R. Hoffmann, W. Balserski, and J. Moss, *2nd NIMS Int. Conf. on Photocatalysis: Fundamental and Applications*; Books of Abstracts, 2004. p. 43.
69. K. Harada, T. Hisanaga, and K. Tanaka, *New J. Chem.* **11**, 598 (1987).
70. K. Harada, T. Hisanaga, and K. Tanaka, *Wat. Res.* **24**, 1415 (1990).
71. M. Abdullah, G. K. C. Low, and R. W. Matthews, *J. Phys. Chem.* **94**, 6820 (1990).
72. C. Guillard, J-M. Herrmann, J. P. Chevrier, C. Bertrand, and E. Philibert (French patent).
73. H. Lachheb, E. Puzenat, A. Houas, M. Ksibi, E. Elaloui, C. Guillard, and J. M. Herrmann, *Appl. Catal. B: Environmental*, **39**, 75 (2002).
74. M. Karkmaz, E. Puzenat, C. Guillard, and J. M. Herrmann, *Appl. Catal. B*, **51**, 183 (2004).
75. J.-M. Herrmann, J. Disdier, and P. Pichat, *Chem. Phys. Lett.* **108**, 618 (1984).
76. P. Pichat, J. M. Herrman, J. Disdier, M.-N. Mozzanega, and H. Courbon, in S. Kaliaguine and A. Mahay, eds., *Catalysis on the Energy Scene*, 1984, p. 319.
77. H. G. Völz, G. Kaempf, H. G. Fitzky, and A. Klaeren, *ACS symp. Ser.*, **151**, 163 (1981).
78. D. M. Blake, in F. Sterrett, ed., *Alternative Fuels and the Environment*, Lewis, Boca Raton, Fla., 1994, p. 175 and Refs. therein.
79. D. Bockelmann, D. Weichgrebe, R. Goslich, D. Bahnemann, *Sol. Energy Mater. Sol. Cells*, **38**, 441 (1995).
80. J. Blanco, S. Malato, and C. Richter, "Solar Chemistry Technology", in *Solar Thermal Test Facilities, Solar PACES Report III*, 1996, chapt. 8, p. 145.
81. D. Curco, S. Malato, J. Blanco, J. Jimenez, and P. Marco, *Solar Energy* **56**, 387 (1996).
82. S. Malato, J. Blanco, C. Richter, D. Curco, and J. Gimenez, *Wat. Sci. Technol.* **35**, 157 (1997).
83. C. Minero, E. Pelizzetti, S. Malato, and J. Blanco, *Solar Energy* **56**, 421 (1996).
84. C. Minero, E. PelizzettiI, S. Malato, and J. Blanco, *Solar Energy* **56**, 411 (1996).
85. R. Goslich, R. Dillert, and D. Bahnemann, *Water Sci. Technol.* **35**, 137 (1997).
86. S. Malato, C. Richter, J. Blanco, and M. Vincent, *Solar Energy* **56**, 401 (1996).
87. S. Malato, J. Blanco, C. Richter, B. Braun, and M. Maldonado, *Appl. Catal B: Environmental*, **17**, 347 (1998).
88. O. Levenspiel, *Chemical Reaction Engineering*, John Wiley & Sons, Inc., New York, 1972, p. 175.
89. C. Guillard, J. Disdier, C. Monnet, J. Dussaud, S. Malato, J. Blanco, M. I. Maldonado, and J. M. Herrmann, *Appl. Catal. B: Environmental* **46**, 319 (2003).
90. European Program AQUACAT: N° ICA3 – CT – 2002-10016 http://aquacat.univ-lyon1.fr/
91. European Program SOLWATER: N° ICA4–CT–2002-10001 http:\\www.psa.es\webeng\solwater\index.html
92. G. L. Fisher, D. P. Y. Chang, and M. Brummer, *Science* **192**, 553 (1976).
93. J. Casado, J. M. Herrmann, and P. Pichat, in P. Borrell, and co-eds., "Transport and Transformation of pollutants in the Troposphere", SPB Acad. Pub BV, The Hague, 1991, p. 307.
94. C. Guillard, H. Delprat, C. Hoang-Van, and P. Pichat, *J. Atm. Chem.* **16**, 47 (1993).
95. H. Wise and K. M. Sancier, *Catal. Lett.* **11**, 277 (1991).

96. J. L. Mansot, J. M. Herrmann, and B. Lasnier, *33*° Colloque Soc.Fr. Microscopie Electronique, Lyon, Book of Abstracts, 1993, p. 38.
97. J. M. Herrmann and J. L. Mansot, *Entropie* **228**, 60 (2000).
98. A. Fujishima, *Look Japan*, **41**, 47 (1995).
99. A. Heller, *Acc. Chem. Res.* **28**, 503 (1995).
100. V. Romeas, Thèse de Doctorat de l'Université Lyon I, n° 98/134, 1998.
101. V. Romeas, P. Pichat, C. Guillard, T. Chopin, and C. Lehaut, *New. J. Chem.* **23**, 365 (1999).
102. R.-X. Cai, K. Hashimoto, K. Itoh, Y. Kubota, and A. Fujishima, *Bull. Chem.Soc. Jpn.* **64**, 1268 (1991).

JEAN-MARIE HERRMANN
Université Claude Bernard Lyon 1

Table 1. **Fine Chemicals vs Environmental Catalysis: Parameters and Characteristics of Photocatalytic Reactions**

Parameters	Fine chemicals	Environmental catalysis
catalyst	TiO_2, Pt/TiO_2	TiO_2
photoreactors	batch, plug flow	batch plug flow
medium	gas and liquid phase	gas and liquid phase
activation process	photonic absorption	photonic absorption
kinetic laws	Langmuir-Hinshelwood	Langmuir-Hinshelwood
main reaction	mild oxidation	total oxidation
initial selectivity	100%	no selectivity
final products for organics	R-CO-R′	CO_2
medium	dry medium	water, humid air
active species	O*	OH°
reaction of formation of the active species	$(TiO_2) + hv \rightarrow e^- + h^+$ $O^-_{(ads)} + h^+ \rightarrow O^-_{(ads)}$	$(H_2O \rightleftharpoons H^+ + OH^-) + h^+ \rightarrow H^+ + OH^\circ$

Table 2. **Illustrative List of Aqueous Pollutants Eliminated and Mineralized by Photocatalysis**[a]

Class of organics	Examples
alkanes	isobutane, pentane, heptane, cyclohexane, paraffins
haloalkanes	mono-, di-, tri- and tetrachloromethane, tribromoethane, 1,1,1-trifluoro-2,2,2 trichloroethane
aliphatic alcohols	methanol, ethanol, propanol, glucose
aliphatic carboxylic acids	formic, ethanoic, propanoic, oxalic, butyric, malic acids
alkenes	propene, cyclohexene
haloalkenes	1,2-dichloroethylene, 1,1,2-trichloroethylene
aromatics	benzene, naphthalene
haloaromatics	chlorobenzene, 1,2-dichlorobenzene
nitrohaloaromatics	dichloronitrobenzene
phenolic compounds	phenol, hydroquinone, catechol, methylcatechol, resorcinol, *o*- *m* -, *p*-cresol, nitrophenols
halophenols	2-, 3-, 4-Chlorophenol, pentachlorophenol, 4-fluorophenol,
amides	benzamide
aromatic carboxylic acids	benzoic, 4-aminobenzoic, phthalic, salicylic, *m*- and
acids	*p*-hydroxybenzoic, chlorohydroxybenzoic chlorobenzoic acids
surfactants	sodium dodecylsulfate, polyethylene glycol, sodium dodecyl benzene sulfonate, trimethyl phosphate, tetrabutylammonium phosphate
herbicides	atrazine, prometron, propetryne, bentazon, 2-4 D, monuron
pesticides	DDT, parathion, lindane,
organo-phosphorus	tetrachlorvinphos, phenitrothion
dyes	mMethylene blue, rhodamine B, methyl orange, fluorescein, Congo Red

[a]A rather complete list of all photocatalytically degradable pollutants has been established by D. Blake, Ref. 11.

Table 3. **Mean Radiant Flux and Rate Constants of 2,4-D Disappearance (k(2,4-D)) and of TOC Elimination (k(TOC)) on Two Different Days**[a]

Date	Φ (W/m^2)	k (2,4-D) (min^{-1})	k (TOC) (ppm/min^{-1})
June 7, 1996	31	6.79×10^{-2}	0.1575
June 13, 1996	38.2	8.72×10^{-2}	0.203
	Φ_7	k_7	$k_{(TOC)7}$
	$— = 0.81$	$— = 0.78$	$— = 0.78$
	Φ_{13}	k_{13}	$k_{(TOC)13}$

[a](June 7th, 1996: partly cloudy; June 13th, 1996: bright sunny). The subscripts 7 and 13 refer to the dates in June 1996.

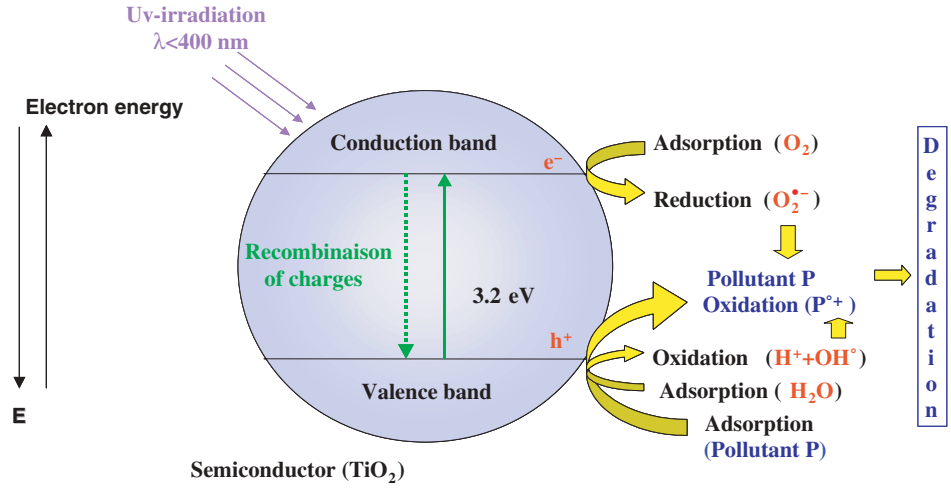

Fig. 1. Energy band diagram of a spherical titania particle.

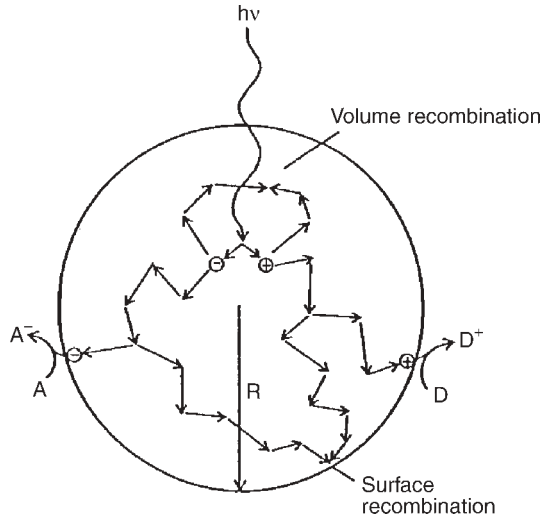

Fig. 2. Fate of electrons and holes within a spherical particle of titania in the presence of an acceptor (A) and (D) molecules (after the late Dr.H. Gerisher, Ref. 12.).

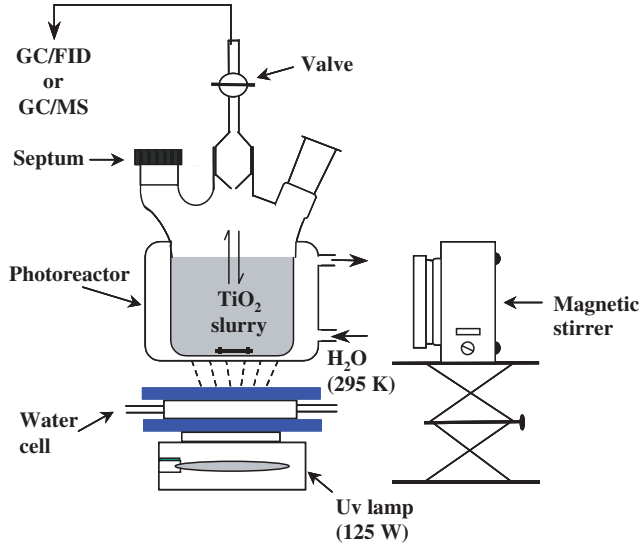

Fig. 3. Scheme of a typical laboratory scale microphotoreactor for the liquid phase using titania in slurry.

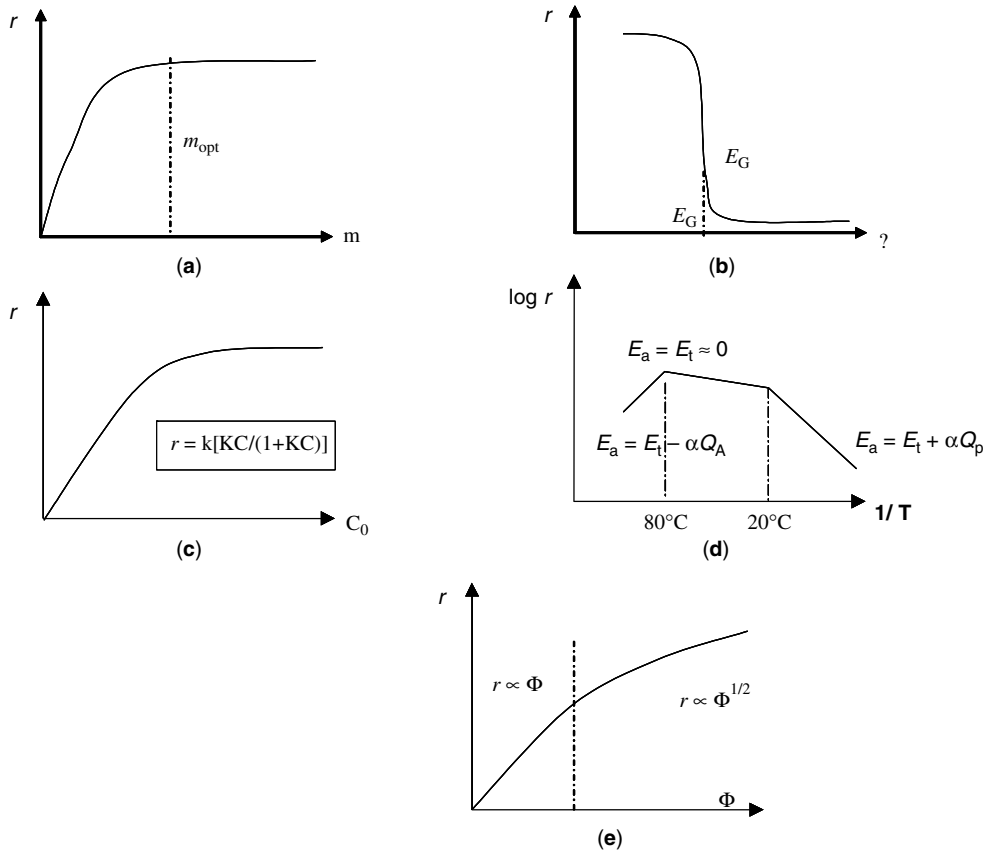

Fig. 4. Influence of the five basic physical parameters which govern the kinetics of photocatalysis: reaction rate r; (**a**): mass of catalyst m: (**b**): wavelength λ; (**c**): initial concentration C of reactant; (**d**): temperature T; (**e**): radiant flux Φ.

$$H_2S + 2\,O_2 \rightarrow SO_4^{2-} + 2\,H+$$

$$SH- + 2\,O^{2+} \rightarrow SO_4^{2-} + H+$$

$$S^{2-} + 2\,O_2 \rightarrow SO_4^{2-}$$

$$SO_3^{2-} + 1/2\,O_2 \rightarrow SO_4^{2-}$$

$$S_2O_3^{2-} + 2\,O_2 + H_2O \rightarrow 2\,SO_4^{2-} + 2\,H+$$

$$NO^{2-} + 1/2\,O_2 \rightarrow NO^{3-}$$

$$NH^{4+} + 1/2\,O_2 + H_2O \rightarrow NO^{3-} + 2\,H_2O + 2\,H+$$

$$H_3PO_3 + 1/2\,O_2 \rightarrow H_3PO_4$$

$$CN^- + 1/2\,O_2 \rightarrow OCN^- \qquad [\,OCN^- + 2\,H_2O \rightarrow CO_3^{2-} + NH^{4+}]$$

Catalysts

$$TiO_2 >> ZnO^* > ZrO_2 > CeO_2 \approx SnO_2 > CdS^* > MoO_3 \approx WO_3 >> V_2O_5 = 0$$

Fig. 5. Photocatalytic decontamination of aqueous solutions containing commons anions. The central element (S, N, P, C) is oxidized to its harmless oxidation degree.

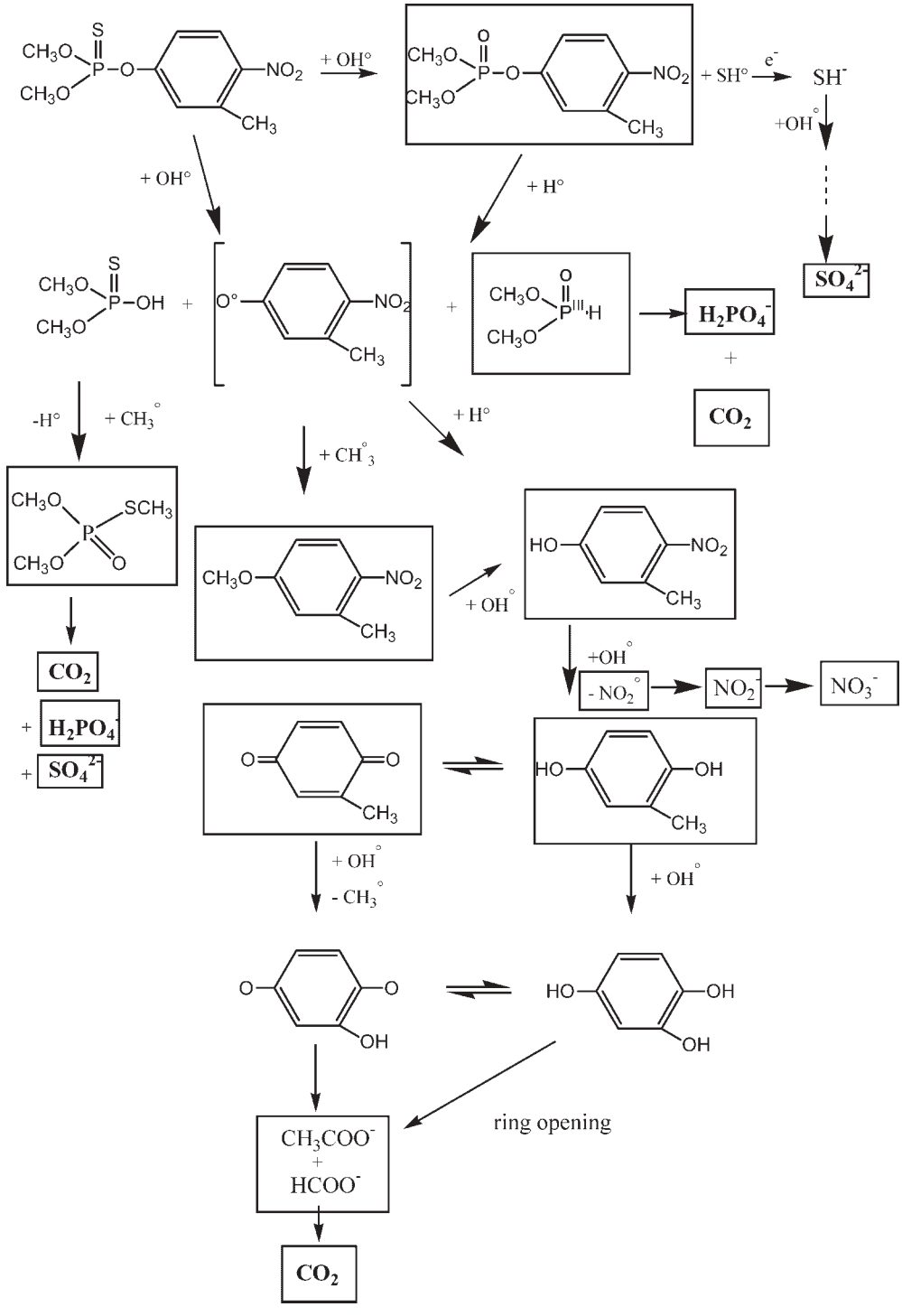

Fig. 6. Photocatalytic degradation pathway of organophosphorus Fenitrothion (the framed molecules correspond to those actually detected).

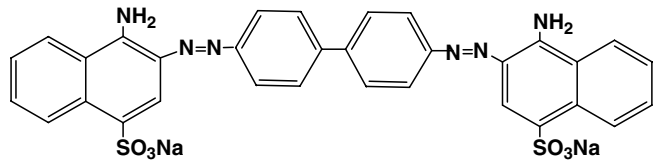

(**a**)

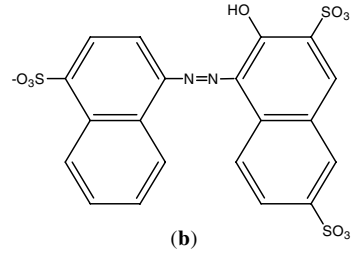

(**b**)

Fig. 7. Developed formulas of two azo-dyes: (**a**) Congo Red (industrial); and (**b**) Amaranth (alimentary).

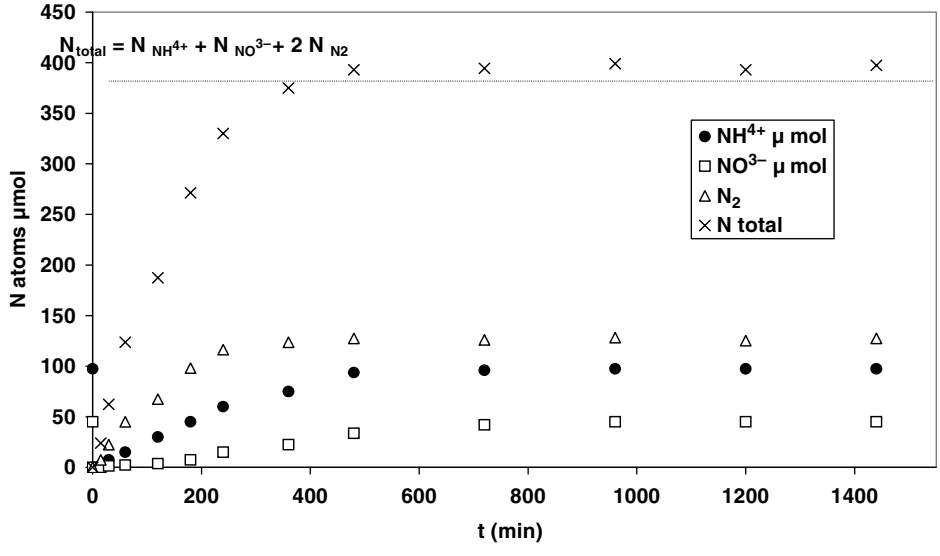

Fig. 8. Kinetics of the evolution of an N-containing compound, either in the aqueous or the gas phase during the photocatalytic degradation of Congo Red dye.

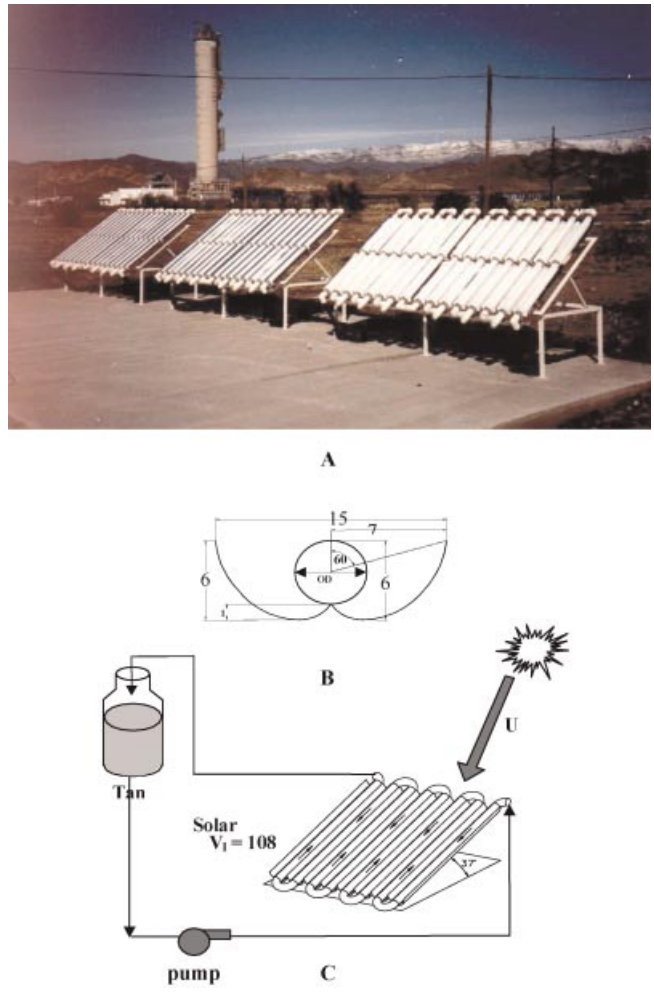

Fig. 9. Scheme of the CPC photoreactor at PSA.

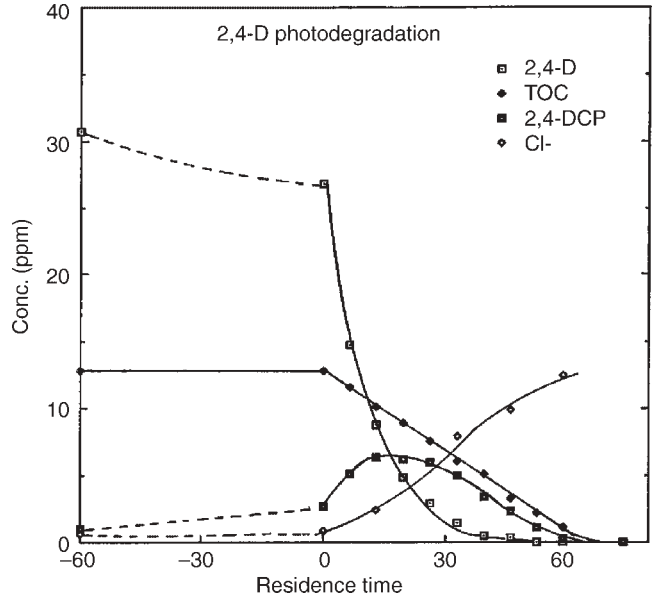

Fig. 10. Kinetics of 2,4-D and TOC disappearance, of Cl^- anion formation and of 2,4-DCP appearance and disappearance.

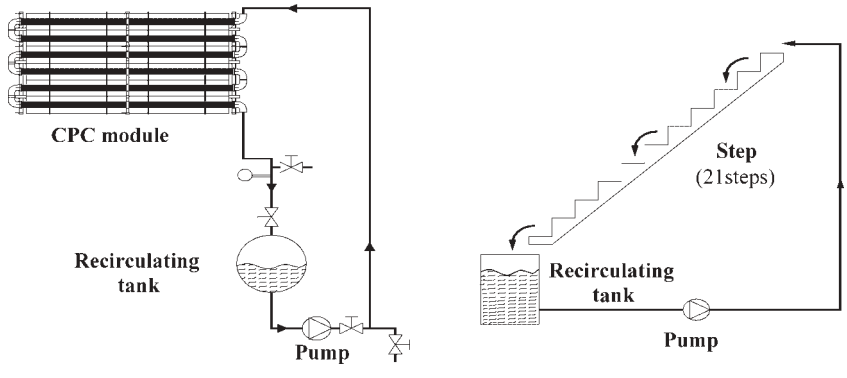

Fig. 11. Comparative schemes of CPC and Cascade falling films photoreactors.

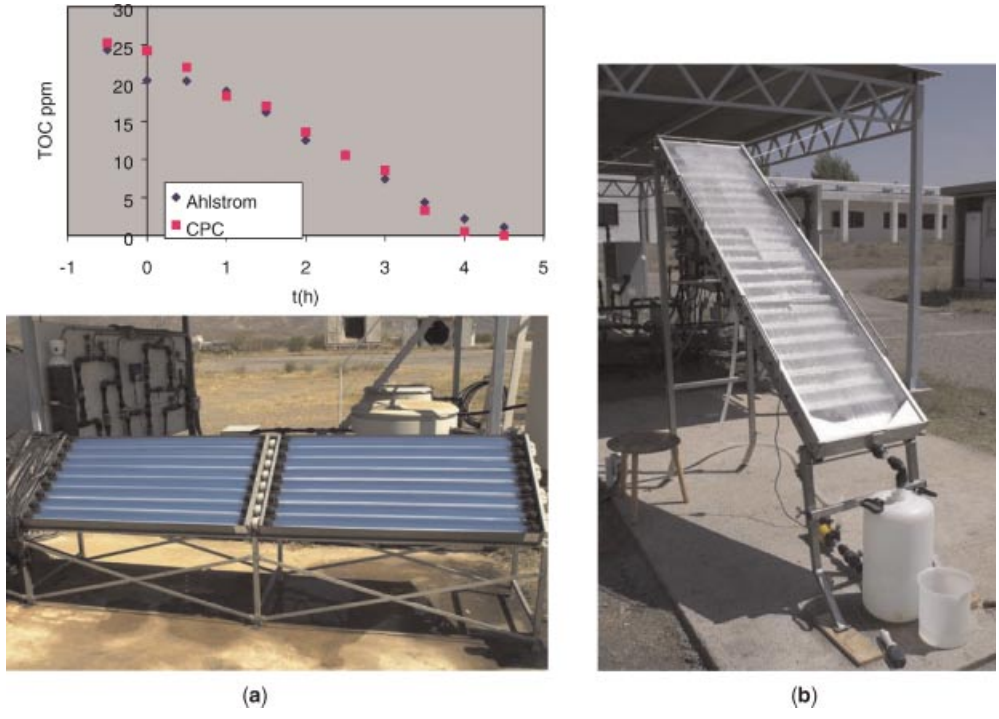

Fig. 12. Comparison of the activities of titania photocatalysts used in (**a**) CPC slurry photoreactor and in a cascade falling films photoreactor using a titania fixed bed deposited on an Ahlstrom paper(**b**).